Original article

On the CMAS Problem in Thermal Barrier Coatings: Benchmarking Thermochemical Resistance of Oxides Alternative to YSZ Through a Microscopic Standpoint

Termal Bariyer Kaplamalardaki CMAS Problemi Üzerine: Mikroskopik Bir Bakış Açısıyla YSZ'ya Alternatif Oksitlerin Termokimyasal Dirençlerinin Kıyaslanması

Çağan Berker İyi [a,*], Martha Mecartney [b] & Daniel R. Mumm [b]

[a] Department of Metallurgy and Materials Engineering, Faculty of Engineering, Kütahya Dumlupınar University, Kütahya, Turkey
[b] Department of Chemical Engineering and Materials Science, University of California, Irvine, USA

Abstract

This study focuses on experimental modelling of the failure of Thermal Barrier Coatings (TBCs) due to the attack of CMAS (Calcia-Magnesia-Alumina-Silicate), which is often found in harsh environments, via glassy phase infiltration. Volcanic ash and dust, sand particles, and fly ash, which contain CMAS, are imminent threats impeding predictable lifetimes of TBCs. Such incurrence directly affects the geometry and clinging to bond coat, and intrinsic material properties such as thermal conductivity and crystal structure of TBC are modified after exposure to CMAS, which ultimately results in delamination, spallation and failure of the coating material. The scope of this work is to survey the reactivity of CMAS with various oxide systems, and to evaluate possible oxide systems that can be replaced and/or used with Yttria-stabilized Zirconia (YSZ) by investigating the penetration depth and reactivity after sintering with CMAS. A cost-effective method to observe the reac-tion of candidate oxides with CMAS is suggested and administired; understanding the main mechanism that causes the failure of top coat in the wake of CMAS infiltration, and seeking solutions for the problem is performed by taking ad-vantage of Scanning Electron Microscopy (SEM). Recently suggested ceramic oxide systems that form in pyrochlore struc-ture, some perovskite structures in various compositions, monazite, mullite and YSZ are studied. The possible outcome consequent upon CMAS infiltration are concluded and course for designing novel material systems that are expected to withstand the CMAS attacks better than the state-of-the-art 4mole% YSZ is defined. 5% mole Yb-doped SrZrO3(5Yb-SZ) and favored pyrochlores such as Gd2r2O7 and GdYbZr2O7 are found to better mitigate CMAS attacks.

Keywords: CMAS, thermal barrier coating, perovskite, pyrochlore, glassy phase infiltration.

Özet

Bu çalışma, termal bariyer kaplamaların (TBC), çetin ortam koşullarında camsı faz infiltrasyonuna sebebiyet veren CMAS (Kalsiya-Magnezya-Alümina-Silikat)'a maruz kalma durumundan kaynaklı bozulmalarının deneysel bir modeli üzerinde yoğunlaşmaktadır. CMAS ihtiva eden volkanik kül, tozlar ve kum parçacıkları TBC'ların tahmin edilebilir servis ömürlerini sekteye uğratmada tehlike arz etmektedirler. Bu şekilde bir CMAS'a maruz kalma durumu, bağ kaplamaya tutunmayı ve geometriyi değiştirmekte, kristal

---

* Corresponding author:

İyi, Çağan Berker is a research assisstant at Dumlupınar University, Faculty of Engineering. His area of interest are processing of advanced ceramics, carbothermic reduction of metals, metal borides, thermal barrier coatings and energy storage materials. He completed his Bachelor's degree in Materials Science and Engineering at Anadolu University in 2007. He received his MS degree in the same field from UC Irvine in 2012.
Email: cabiyi@gmail.com

yapının değişimi ile birlikte temal iletkenlik gibi içsel malzeme özelliklerini modifiye etmekte ve kaplama malzemesinin nihai olarak tabakalanması, parçalanması ve bozulmasına sebebiyet vermektedir. Bu çalışmanın kapsamı, CMAS'ın çeşitli oksit sistemleri ile reaktivitesini gözlemleyerek yitria-stabilize zirkonya (YSZ) yerine/veya birlikte kullanılabilecek uygun oksit sistemlerin CMAS ile sinterleme sonrası penetrasyon derinliğini tespit etmektir. Aday oksitlerin CMAS ile reaksiyonunun gözlemlenmesi için düşük maliyetli bir yöntem önerilmiş ve uygulanmıştır; üst kaplamanın CMAS'tan dolayı bozulmasındaki temel mekanizmanın anlaşılması ve bu soruna çözüm önerilerinin getirilmesi Taramalı Elektron Mikroskobu (SEM) yardımı ile gerçekleştirilmiştir. Yakın zamanda önerilen bazı payroklor ve perovskit oksit sistemleri, monazit, müllit ve YSZ üzerine çalışılmıştır. CMAS infiltrasyonu sonucunda olası sonuçlar özetlenmiş ve son teknoloji 4 mole% YSZ'dan daha dayanıklı yeni malzemelerin geliştirilmesi yönünde izlenmesi gereken yollar tanımlanmıştır. 5% mol Yb-doplu SrZrO3(5Yb-SZ) perovskitin ve Gd2r2O7, GdYbZr2O7 gibi tercih edilen payroklor yapıların CMAS'ın etkisini azaltmada daha başarılı olduğu gözlemlenmiştir.

Anahtar Kelimeler: CMAS, termal bariyer kaplama, perovskit, payroklor, camsı faz infiltrasyonu.

INTRODUCTION

Gas turbines, which are indispensable energy sources for jet propulsion, power generation, and marine propulsion, have been thermodynamically proved to be providing significantly higher power with respect to increasing temperature [1]. Increasing the gas inlet temperatures in the combustion chamber, thereby, results in higher efficiency; however, it ultimately affects the turbine components in the chamber. Gas turbine engine is a highly complicated structure, which consists of various sections. Thermal Barrier Coatings (TBCs), which participate in the hot-section of gas turbines, are the insulating coatings that attenuate the surface temperature by 100-300°C [2], protect turbine blades from environmental effects, and provide cleaner exhaust [3].

TBC systems consist of three major components: a) the metallic bond-coat (BC), (b) the thermally grown oxide (TGO), (c) the ceramic top coat (shown in Figure 1). The bond coat is usually an aluminum rich metal alloy that is known as MCrAlY [4,5], where M stands for Co, Ni or NiCo. The bond coat layer takes part on the substrate (superalloy) by bonding onto with a compatible thermal expansion coefficient to that of the superalloy. TGO layer is the region where dense layer of α-Al_2O_3 is formed which is usually <10μm [6]. This part of the TBC comprises significant part of the technology, because most of the failures take place in this region (mostly TBC/TGO interface) via various mechanisms [6-14]. Regardless, alumina is desired due to its low oxygen diffusivity and superior adherence [15]. The top coat, which is a ceramic layer, is the main concern of this study since surface of the top coat is where the most important interactions with the environment take place.
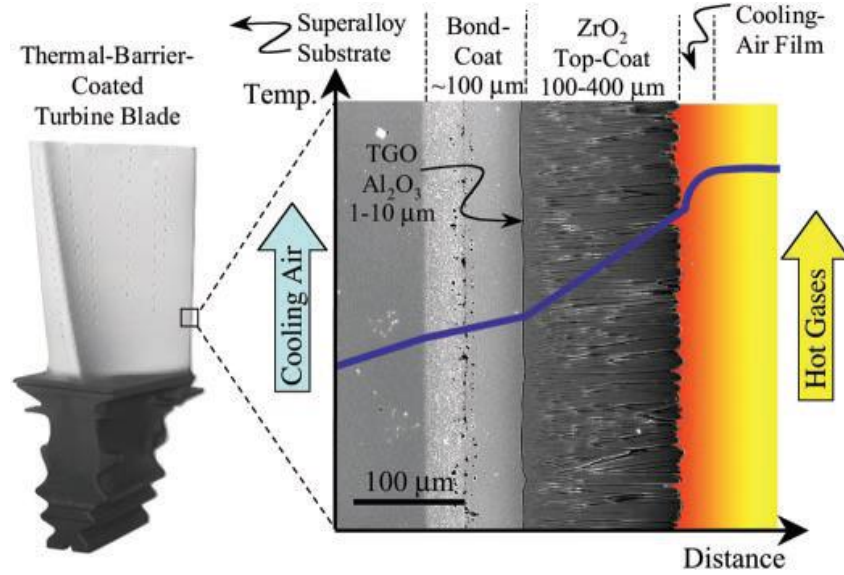
Figure 1. A schematic illustration of a modern thermal barrier coating system consisting of a ceramic top coat, a thermally grown oxide (TGO) and an aluminum rich bond coat. Temperature gradient is indicated with the blue line (From Padture et al. Science 296 280-284 (2002) [2]).

The most commonly used ceramic oxide material for TBCs is ZrO_2 doped by Y_2O_3. The reason for using this system (or other divalent or trivalent cations' oxides) arises from its outstanding results due to the metastable tetragonal (denoted by *t'*) phase that provides excellent properties such as compatible coefficient of thermal expansion, high toughness, and most importantly, phase stability at all temperatures within the operation range (273-1773ºK). This metastable phase exists within 3.7-7 mole% Y_2O_3 dopant amount, which was first discovered by Garvie, Hannick and Pascoe in 1975 [16], and soon verified to be the most desired crystal structure of the potent candidate YSZ in 1976 [17,18]. State-of-the-art coating serving as TBC for over a quarter century is 4 mole% yttria-stabilized zirconia (4YSZ), which was suggested by a NASA employee, Stephan Stecura, who found the most ideal stoichiometry (the exact composition is ~ 3.7 mole%) for TBC applications in 1985 [18].

There is an increasing interest in research and development of TBCs within the last decades. In order to select convenient material systems for TBC applications, one should consider all these additional factors besides a compatible coefficient of thermal expansion (CTE) and low thermal conductivity [2]:

1. Phase stability: The crystal structure and the desired phase of the top coat must remain the same in the range of 273-1573°K (operating temperature)

2. Corrosion/Erosion resistance: Some salts such as Na_2SO_4 and V_2O_5 that attack to the top coat have a deleterious effect at operating temperature [19]. TBCs are expected to be withstanding so-called 'hot corrosion' and mechanical impacts that lead to erosion.

3. Durability: Long-term durability is desired.

4. Adherence: The adherence of the top coat to the bond coat is vital.

5. Morphological stability: The morphology of the top coat is expected to be stable. Otherwise, alteration in morphology might cause disruption in strain tolerance and excessive sintering.

6. Strength/Toughness: High specific strength that will tolerate the stretching and contracting for a long service time is desired.

7. Resistance to oxygen diffusion: Oxygen transparency is a serious problem, which results in transportation of oxygen to the TGO layer, and ultimately to the bond coat.

This is a challenging pursuit of optimization for a material system when all these factors come into play. Thereby, it is possible to say that TBC is one of the most complicated material systems when this complexity of desired properties taken into account. Clarke [20] suggested that there are three major concerns in searching for a candidate material for TBCs, which are: i) Selecting oxides with low thermal conductivity; ii) controlling the internal porosity by means of creating and stabilizing pores for reducing heat transfer; iii) estimating the thermodynamical stability with α-alumina in TGO. The most arduous pursuit among these is the latter one, which is how to estimate the thermodynamical stability with alumina, according to Clarke.

Especially in the last two decades, there has been a concerted effort to study YSZ and pertinent TBCs and their susceptibility to environmental deposits [21-35]. These deposits that are ingested into the hot engine during service usually consist of calcium, magnesium, aluminum, and silicon oxides (CMAS), common constituents often found in fly ash, volcanic dust particles and sand. The results of these studies show that CMAS constitutes a remarkable problem, and it cannot be ignored. Substantial observations on the penetration mechanisms of CMAS in YSZ TBCs have been made, and correlations between susceptibility of TBCs to CMAS attacks and the phase stability of the YSZ structure have been found. However, a complete understanding in regards to the interaction of the top coat with CMAS with respect to compositions still remains vague. Understanding the reaction of CMAS with the other potential candidate oxides is essential in order to design new generation thermal barrier systems.

CMAS —typically made for the laboratory with a composition of 33-9-13-45 cation mole% of Ca-Mg-Al-Si— is known to melt and form a glassy phase around 1240°C [20]. When melting takes place, it infiltrates into the TBC material via columnar pore channels or open porosities (for EB-PVD deposited and APS coated TBCs, respectively) and undergoes a serious of chemical reactions with the oxide TBC [21]. Borom et al. [22] reported the first known study on malignant consequences of CMAS on TBCs in 1996 when they realized the helicopter rotor blades and paddles suffer from Saudi Arabian sand deposits. They adduced that the problem emerges from infiltration of the molten glassy phase into the open void space in TBCs, which is caused by the capillary pressure, as a result of the electron microprobe analysis they carried out. Their results indicate that CMAS generally forms diopside

$(MgCaSi_2O_6)$, and the melting range and the freezing range of CMAS deposits was found to be varying dependent on the initial composition [22]. In 2006, thermochemical interaction of TBCs with CMAS was explained by Krämer et al. [21, 24]. They adduced that the phase transformation of YSZ is triggered by dissolution in the CMAS glass that reduces the yttrium content in the YSZ. This non-transformable tetragonal (*t'*) to monoclinic transformation results in an expansion of 4.7%, by volume [36]. By this approach, the phenomenon acquires a new dimension that phase stability of YSZ is one of the most significant concerns. YSZ was already known to be undergoing phase transformation with silicates. However, the theoretical calculations by taking advantage of Hollomon-Jaffe parameter in regards to *t'* or *t''* → monoclinic transformation has gained more significance in terms of designing yttria-stabilized zirconia coatings for various applications [37].

MATERIALS and METHODS

Model Geometry

In order to understand the mechanism of CMAS attack on the oxide system of interest, a model that is based on 'center-oriented diffusivity' of CMAS is employed. To examine the penetration mechanism of CMAS, infiltration of the glassy phase is observed via evaluating the cross-section of the pellets after sintering with CMAS. For this purpose, the pellets were bisque-fired at a low temperature (1050°C) so that they have open porosity to accommodate the glassy phase. Pore geometry (vertical in TBCs) is not something that can easily be controlled for the pellets obtained with traditional pressing methods. Although it is difficult to estimate the pore size and geometry in these pressed and bisque-fired pellets, in light of the information acquired from density measurements, it is possible to approximate the percent porosity. The target value for the porosity was determined as ~40% in order to achieve bodies as porous as possible. Volumetric measurements were carried out after pressing, cold isostatic press (CIP) was employed for achieving the targeted density, and after bisque-firing, Archimedes method was utilized.

Figure 2 schematically summarizes the methodology employed in this study. The reason for carrying out bisque-firing step is to achieve sufficient mechanical resistance for drilling. The pellets were drilled to a depth of half their thickness; CMAS powder was placed in this divot. Sintering with CMAS was carried out afterwards, which took place at 1300°C for 3 hours. As the last step, the pellets were cross-sectioned by the help of a low speed diamond saw. Cross-sectioned specimens were mounted in epoxy molds, and they were taken out afterwards the epoxy was hardened.
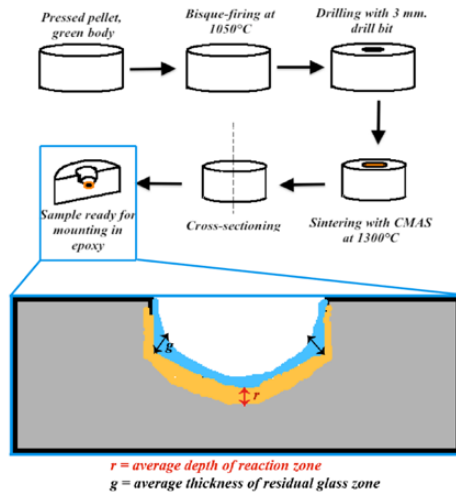
Figure 2. The flowchart of the experiment and defining the terms for nomenclature for the average CMAS penetration depth (r), and average thickness of the CMAS residual glass: i) The pellets are uniaxially pressed using 13 mm. press, ii) Bisque-fired at 1050ºC for 2 hr., iii) Drilling with 3mm. drill bit, iv) Placing the CMAS powder and sintering at 1300ºC for 3hr., v) Cross-sectioning, vi) Mounting in epoxy for SEM characterization.

Porosity concentration and concentration distribution might cause serious deviations in this method. Therefore, controlling the pore geometry and size is important. In order to obtain a high surface quality on the divots, drilling was performed by 3 mm tungsten carbide drill bits. Subsequently, each divot (50μL) was filled with distilled water by taking advantage of high precision pipetting. Specimens that conserve the water on the level with the surface were preferred for infiltration experiments.

Selection of the Oxide Systems of Interest

Nine oxide systems that meet the criteria declared by Padture et al [2] are chosen. Thermal properties of these oxides are given in Table 1 concurrently with 4YSZ. Some of the theoretical data calculated via crystallographic unit cell based approach is indicated as "calculated". All powders were procured commercially except two pyrochlore systems $Gd_2Zr_2O_7$ (GZO) and $(Gd_xYb_{1-x})Zr_2O_7$ (GYZO) with $x=0.5$, which were solid-state synthesized.

Table 1. Some useful properties of the oxide materials that are studied in this work.

Ceramic Oxide	Theoretical density (g cm^{-3})	Thermal expansion coefficient (10^{-6} °K^{-1})	Thermal conductivity (W m^{-1}°K^{-1})	Melting temperature (°C)
4 YSZ	6.03 (calc.)	10-11 [38] (800-1200°C)	1.9-2.3 [20] (30-1200°C)	2700 [39]
Monazite (LaPO$_4$)	5.13 [40]	9.6 [40] (25-1000 °C)	1.25-2 [20] (400-1000°C)	2072±20 [40]
Mullite	3.16 [41]	5.3 [39] (20-1000°C)	3.15-4.63 [20] (25-1000°C)	1850 [39]
BaZrO$_3$	6.24 (calc.)	8.1 [39] (30-1000°C)	3.42 [39] (1000°C)	2690 [39]
CaZrO$_3$	4.95 [42]	11.5 [42] (25-1000°C)	1.22 [43] (400-1400°C)	2330 [42]
SrZrO$_3$	5.53 [44]	10.9 [39] (30-1000°C)	2.08 [45] (1000°C)	2800 [39]
ZrSiO$_4$	4.85 (calc.)	4.99 [46] (27-1427°C)	3.56 [48] (92-1537°C)	1660 [47] (decomp.)
Gd$_2$Zr$_2$O$_7$ (GZO)	8.82 (calc.)	10.5-12 [49] (800-1200°C)	1.45-1.55 [20] (400-1400°C)	2550 [41]
GdYbZr$_2$O$_7$ (GYZO)	9.17 (calc.)	9.6-11.9 [50] (200-1200°C)	1.3-1.5 [50] (400-1400°C)	unknown
5 mol% Yb-SrZrO$_3$ (5 Yb-SZ)	5.76 (calc.)	9.2-10.6 [51] (200-1100°C)	1.5-2 [51] (0-1400°C)	unknown

Solid-State Synthesis of Pyrochlores

In order to obtain Gd$_2$Zr$_2$O$_7$ (GZO) and (Gd$_x$Yb$_{1-x}$) Zr$_2$O$_7$ (GYZO) with $x = 0.5$ –taking Liu et al.'s study as reference– [50], solid-state synthesis was employed. Gd$_2$O$_3$ powder with 99.999% purity (AlfaAesar) and ZrO$_2$ with 99.5% purity (AlfaAesar) were used for GZO and GYZO. For GYZO, Yb$_2$O$_3$ powder with 99.998% purity (AlfaAesar) was employed additionally. Powders were weighed and mixed in the ball mill using ethanol for 24 hours. ZrO$_2$ balls were chosen as the milling media. Once ball milling was completed, the solid solution in ethanol dried in a drying furnace for 8 hours and the powder was milled in the mortar. 13 mm. press was used in order to press the pellets, and two pellets were obtained for each composition. For each composition, one pellet was CIPed whereas the other pellet was direct bisque-fired. Both of these pellets were sintered at 1450°C for 20 hours with a heating rate of

5°C/min. Succeeding formation of pyrochlore structures, the pellets were ground in order to obtain GZO and GYZO powder.

RESULTS and DISCUSSION

This study attempts to present a simulative approach in terms of estimating the CMAS infiltration resistance of candidate oxides applicable in TBCs even though the real circumstances embrace much more complicated factors such as huge centrifugal forces and thinner/heavier atmospheric conditions during the service time. Moreover, EB-PVD (electron beam physical vapor deposition) or APS (atmospheric plasma spray) coated TBCs have a distinct morphology in contrast to pressed pellets used in this study. Nonetheless, experimental results obtained in this study fairly match the results obtained by the specimens exposed to real condition cases presented in the literature [26, 52-54].

X-Ray Diffraction Studies

X-ray diffraction (XRD) results for the solid-state synthesized GZO and GYZO are given in Figure 3. *hkl* indices on the $Gd_2Zr_2O_7$ and $GdYbZr_2O_7$ diffraction patterns are indicated. Siemens D-5000 Diffraktometer model was used at 40 kV voltage and 30 mA current with Cu k_α radiation source with a wavelength of $\lambda = 1.5408$ Å.

Pyrochlores form in isometric crystal system which is in favor of their crystallographic characterization via XRD. XRD results support the solid-state syntheses of GZO and GYZO compositions were successfully achieved, and the transformation was completed thoroughly. The lattice parameter of GZO is calculated as 10.52 Å whereas this value slightly varies to 10.42 Å for GYZO due to the peak shift to the right. This is an expected result owing to the smaller radius of Yb^{3+} ion in 8-fold coordination.
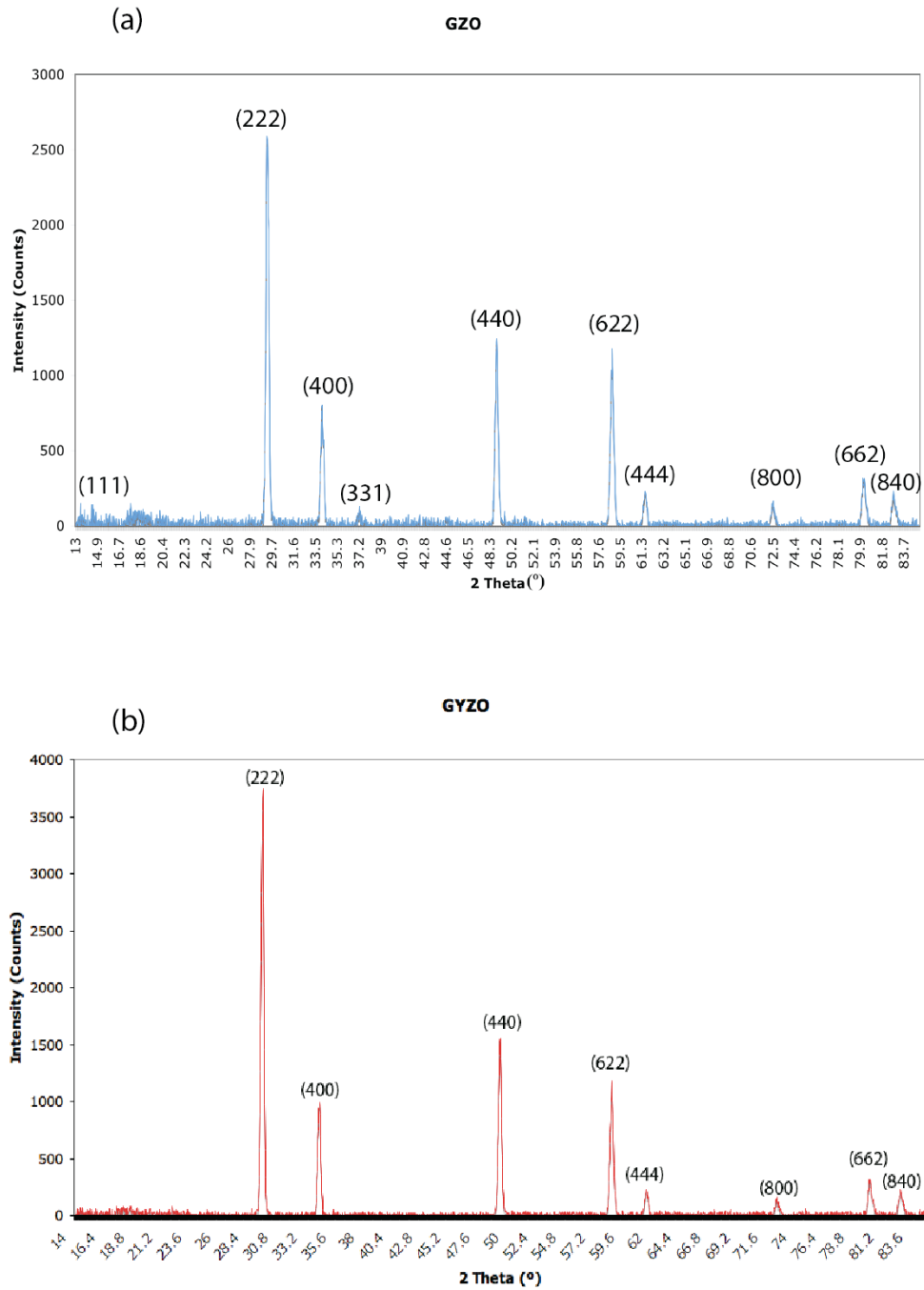
Figure 3. XRD graphs taken from solid-state synthesized pyrochlores: a) GZO and b) GYZO.

Density Calculations

Archimedes' method is employed in order to determine the mean density (ρ) using 5 specimens per each composition. 60% targeted density after bisque-firing at 1050°C is achieved with a slight variance (±5%). After CMAS infiltration (at 1300°C), mean density is calculated which exhibits a wide divergence. Table 2 summarizes Mean density and ρ/ρ_{th} for the specimens obtained by Archimedes' method.

Table 2. Mean density and ρ/ρ_{th} for the specimens obtained by Archimedes' method.

Specimen	Mean ρ after BF (g cm^{-3}) / ρ/ρ_{th} (%)	Mean ρ after sintering with CMAS (g cm^{-3}) / ρ/ρ_{th} (%)
4 YSZ	3.36 / (56%)	5.89 / (98%)
Mullite	1.77 / (56%)	2.57 / (81%)
Monazite	2.85 / (55%)	4.15 / (80%)
BaZrO$_3$	3.63 / (58%)	3.81 / (61%)
CaZrO$_3$	2.91 / (59%)	3.29 / (69%)
SrZrO$_3$	3.18 / (58%)	3.36 / (61%)
ZrSiO$_4$	2.95/ (61%)	3.04/ (63%)
Gd$_2$Zr$_2$O$_7$	4.92 / (56%)	4.97 / (57%)
GdYbZr$_2$O$_7$	6.05 / (66%)	6.08 / (66%)
5 Yb-SZ	3.52 / (61%)	4.55 / (79%)

Infiltration Experiments

An overview in regards to infiltration behavior of specimens is presented in Figure 4. The control sample (4YSZ) is shown first (a) and compared to 5Yb-SZ (on b), which gives the best results in terms of resistance to CMAS. c) and d) represent GZO and GYZO respectively, and e) stands for mullite, f) is monazite, g) Zircon, and h) CaZrO$_3$, i) belongs to SrZrO$_3$ and j) represents BaZrO$_3$, which shows the most vulnerable behavior against CMAS infiltration. Among these oxides, owing to their sufficient resistance, only Yb-SZ, GZO, GYZO and mullite are characterized under SEM through EDS mapping.
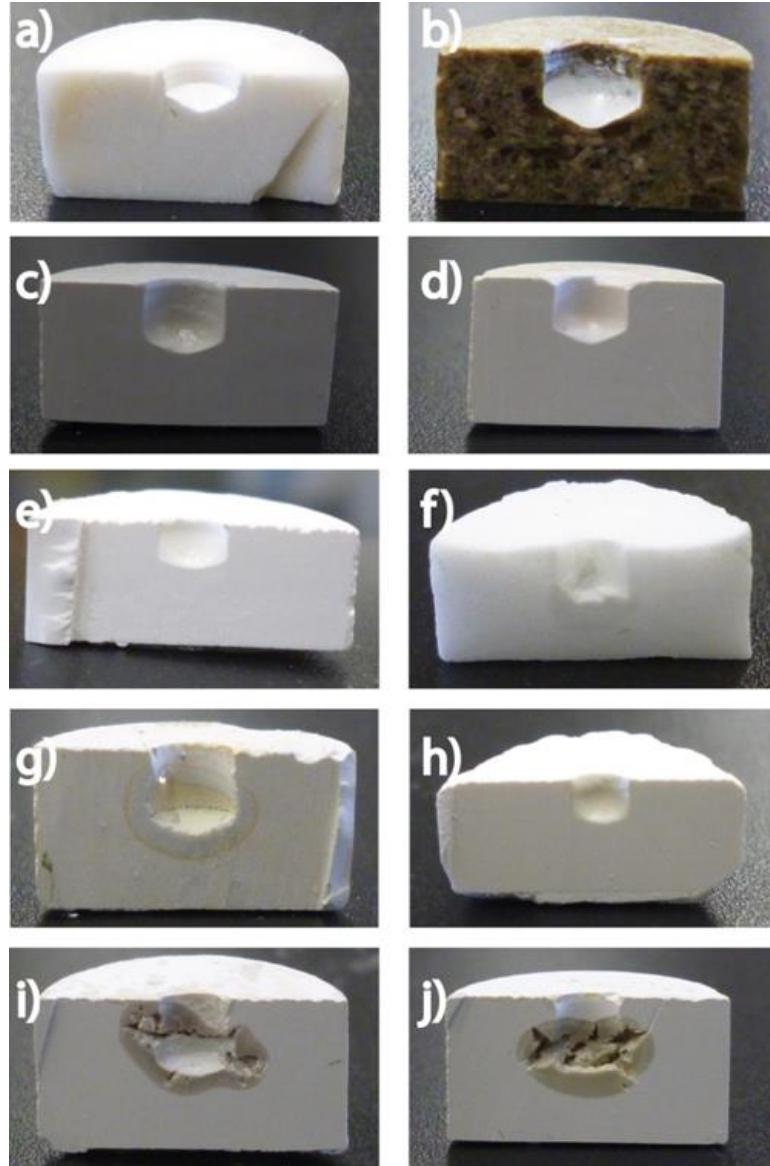
Figure 4. Digital images from the cross-sectioned pellets after sintering with CMAS at 1300°C: a) 4YSZ, b) 5Yb-SZ; c) GZO, d) GYZO, e) Mullite, f) Monazite, g) $ZrSiO_4$, h) $CaZrO_3$, i) $SrZrO_3$, j) $BaZrO_3$.

Oxide Structures of interest that are applicable to TBCs are investigated after CMAS infiltration and three different scenarios for interaction type are defined. Figure 5 summarizes the infiltration behavior of 6 samples representing 3 different possibilities: 4YSZ (no glassy phase), GZO, GYZO and 5 Yb-SZ (glass formation and blocking CMAS in the interaction zone) and degradation of the whole specimen (monazite).
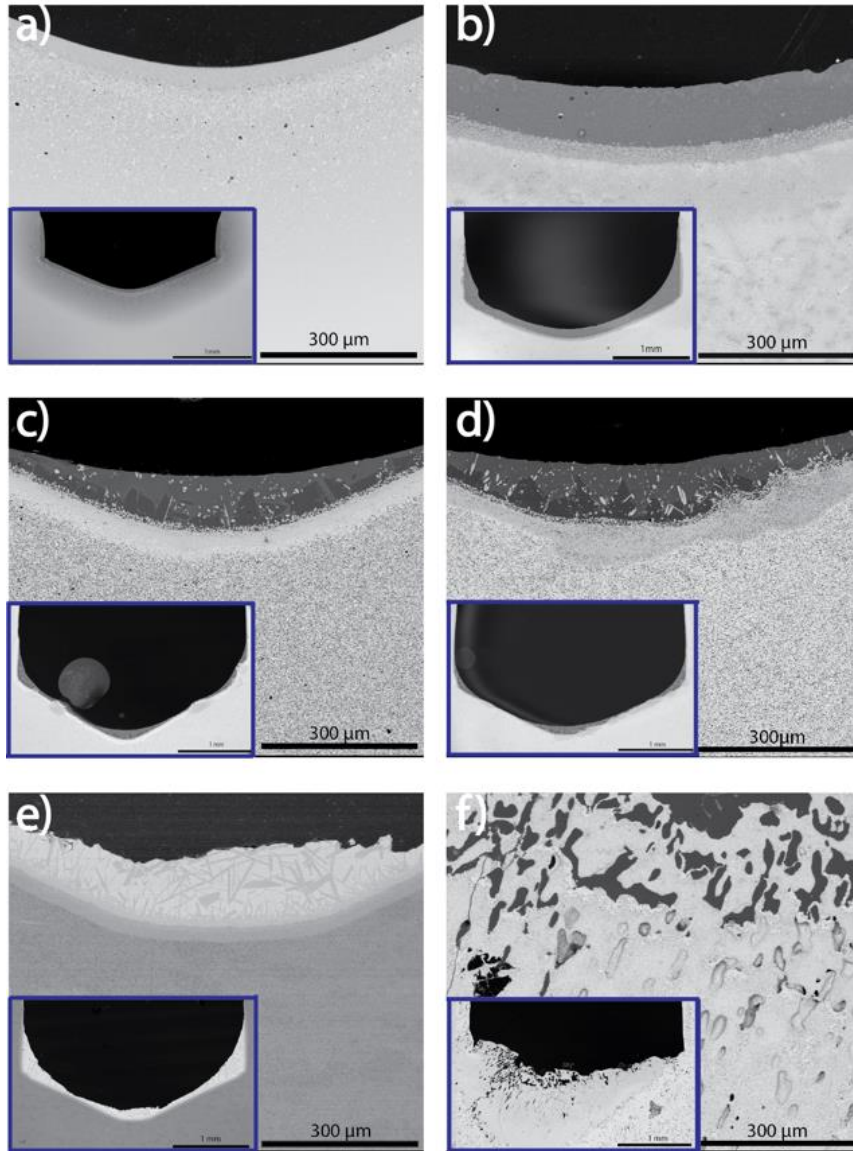
Figure 5. SEM images from the cross-sectioned specimens showing the infiltration region (reaction zone) and the glass layer CMAS formed (for mullite, GZO, GYZO and Yb-SZ). a) 4YSZ, b) 5Yb-SZ, c) GZO, d) GYZO, e) mullite, and f) Monazite.

Figure 6 draws a comparison between the candidate oxides in a graphical abstract where average penetration depth of CMAS (*r*) and average thickness of the residual CMAS glass (*g*) in microns are designated. Figure 7 represents a remarkable example concerning how crystals form in CMAS glass. Uniaxial anorthite ($CaAl_2Si_2O_8$) crystals grow in CMAS glass as expected due to the existence of several eutectics in $CaO-SiO_2-Al_2O_3$ system in the 1200-1300°C range. Mullite specimen gives outstanding results in terms of blocking CMAS infiltration. EDS results also confirm this formation (Figure 8). Mg^{2+} and Ca^{2+} cations are effectively blocked over the interaction zone. However, due to low coefficient of thermal expansion of mullite, EBC (environmental barrier coating) application might be more suitable instead of TBC.
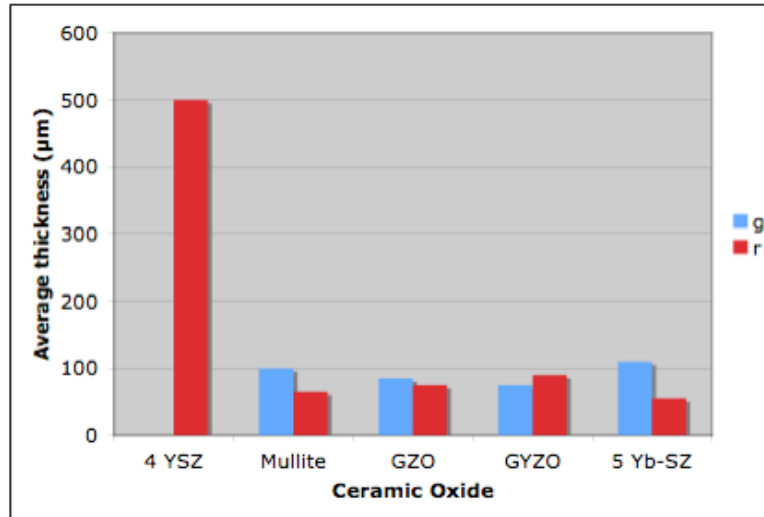
Figure 6. Average penetration depth of CMAS (*r*) and average thickness of the residual CMAS glass (*g*) in microns.
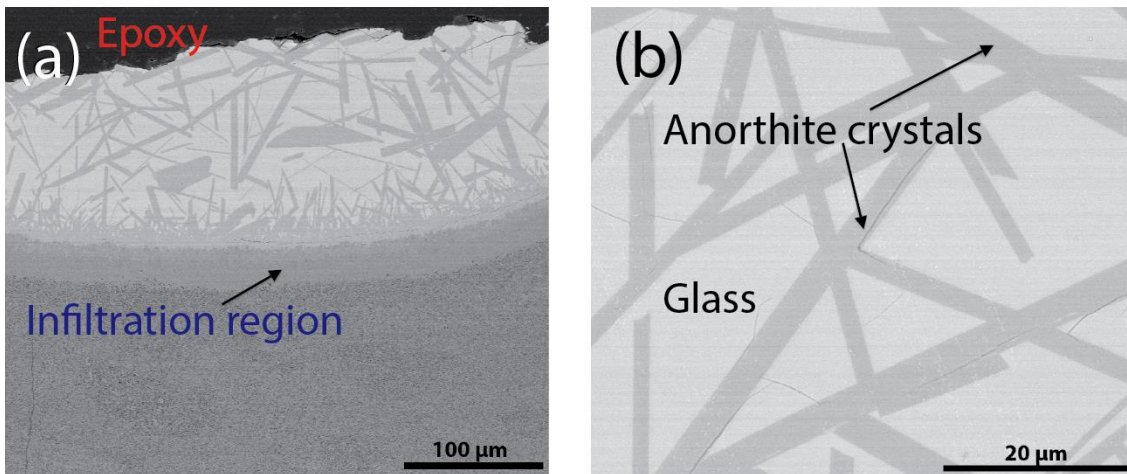
Figure 7. (a) A BSE image from the cross-sectional area that CMAS infiltration into the mullite specimen took place, (b) A BSE image acquired from the glassy region showing anorthite crystals grown in the glass.

There is significant densification in the mullite and monazite pellets when CMAS is introduced. For 4 YSZ, same densification can be obtained regardless of CMAS, which might be due to the quality of the powder used with a very fine particle size of 80 nm. Alternatively, mullite pellets manifest a tremendous densification in contrast to other specimens, which can be explained by transient liquid phase sintering. The crystals grown in CMAS glass are envisaged to be anorthite ($CaAl_2Si_2O_8$). Mullite clearly formed a potent barrier against CMAS infiltration. The glassy phase CMAS creates at 1300°C plays a very important role in sintering due to change in diffusion mechanism. Therefore, it is possible to say that introducing CMAS of 0.001% in mass has enhanced the overall diffusion mechanism.
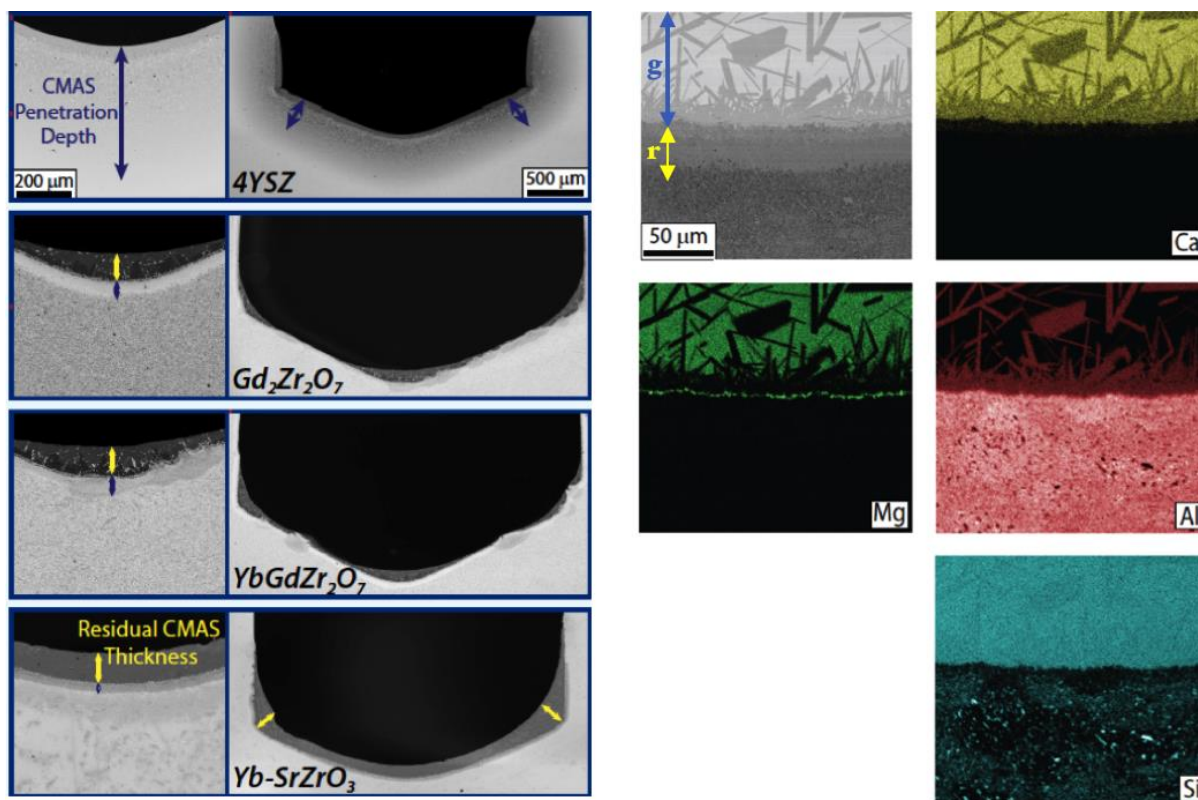
Figure 8. on the left: Comparing the infiltration behavior of CMAS on the oxide structures of interest with the control sample; on the right: EDS mapping results from the mullite specimen.

The color change in some specimens (4YSZ, 5 Yb-SZ) points out that color centers have been altered via defects. The translucent structure of the 4YSZ pellet shows that sample is very dense. Solid-state synthesis of 5 Yb-SZ created a significant color change, too. Both GZO and GYZO pellets showed excellent resistance against CMAS infiltration. 5 mole% Yb-doped $SrZrO_3$ gave the best results in terms of impeding CMAS infiltration. CMAS melt stayed on the surface and solidified leading to glass formation and no cations relating to CMAS has been found in the structure. This result makes 5 mole% Yb-doped $SrZrO_3$ a promising material for the next generation CMAS-Resistant TBCs. Monazite undergoes a different type of reaction with CMAS yielding two different products without bonding (the frit-like debris in the divot and deformed specimen), and exhibits vulnerable behavior against CMAS infiltration.

As a strong representative of potential pyrochlore oxides that are suitable for TBCs, GZO gives promising results. CMAS formed a glass composition and non-stoichiometric crystals where the constituents of GZO dissolved in these phases by forming mainly two structures: Gd rich particles that have the hexagon geometry and mostly form in the glass, and Zr rich spheroids that precipitate just above the interaction region, mainly in these non-stoichiometric crystals. These results indicate that GZO is a strong candidate material that withstands CMAS attacks with effective blocking of the cations even though Mg^{2+} diffuses slightly more than the other cations. Al^{3+} cation, exhibits diffusivity in GYZO in contrast to GZO, where superseding with Yb^{3+} cations is possible. Identically, Si^{4+} cations tend to

take place of Zr^{4+}, which diffuse into the glass formed by CMAS. Yielding substantially similar results to GZO, GYZO also shows fairly favorable resistance to CMAS penetration. However, the infiltration field is not very homogenous, which is probably resulting from the non-uniform porosity. There is a significant amount of nonuniformity in the interaction field, therefore the thickness of the interacted areas vary markedly depending on the position. Figure 9 represents the EDS mapping results concerning the GZO and GYZO comparatively.
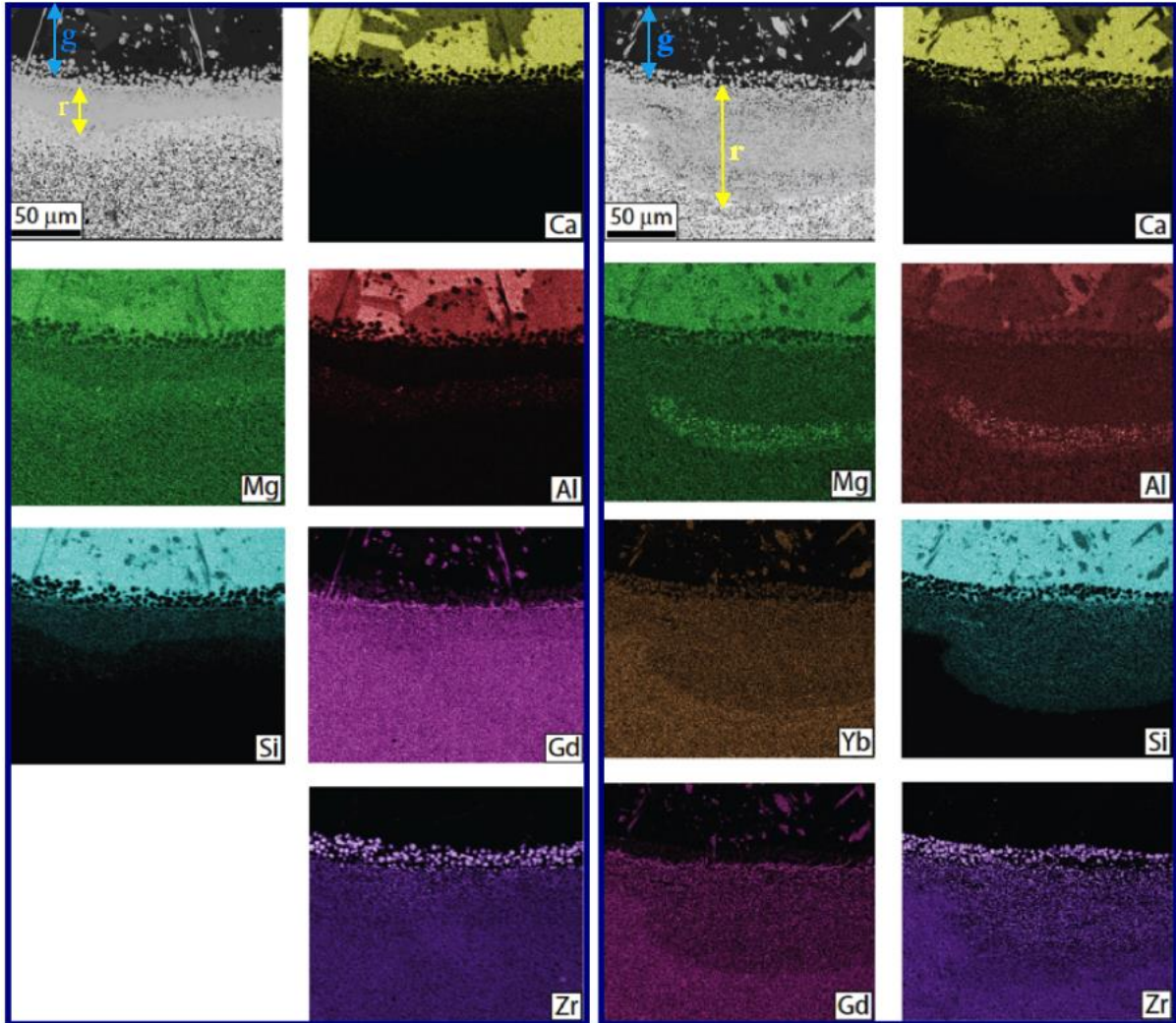
Figure 9. EDS mapping results from the GZO (on the left) and GYZO (on the right) specimen.

Among the oxide systems evaluated in this study, 5 mole% Yb_2O_3 doped $SrZrO_3$ gives the most optimal results. CMAS penetration is less than 30 μm, which results in solidification of most of the CMAS glass in the divot uniformly without interacting with the material. The cations found under the infiltration region are Al^{3+} and Si^{4+}. Sr^{2+} cations show a strong shift from the interaction region towards the surface in order to participate in the glassy phase, probably resulting from its tendency towards

decomposing to SrO and ZrO_2. Sr is depleted in the interaction zone, dissolving into the glass while ZrO_2 precipitated. Figure 10 exhibits the EDS mapping results from the 5Yb-SZ specimen.
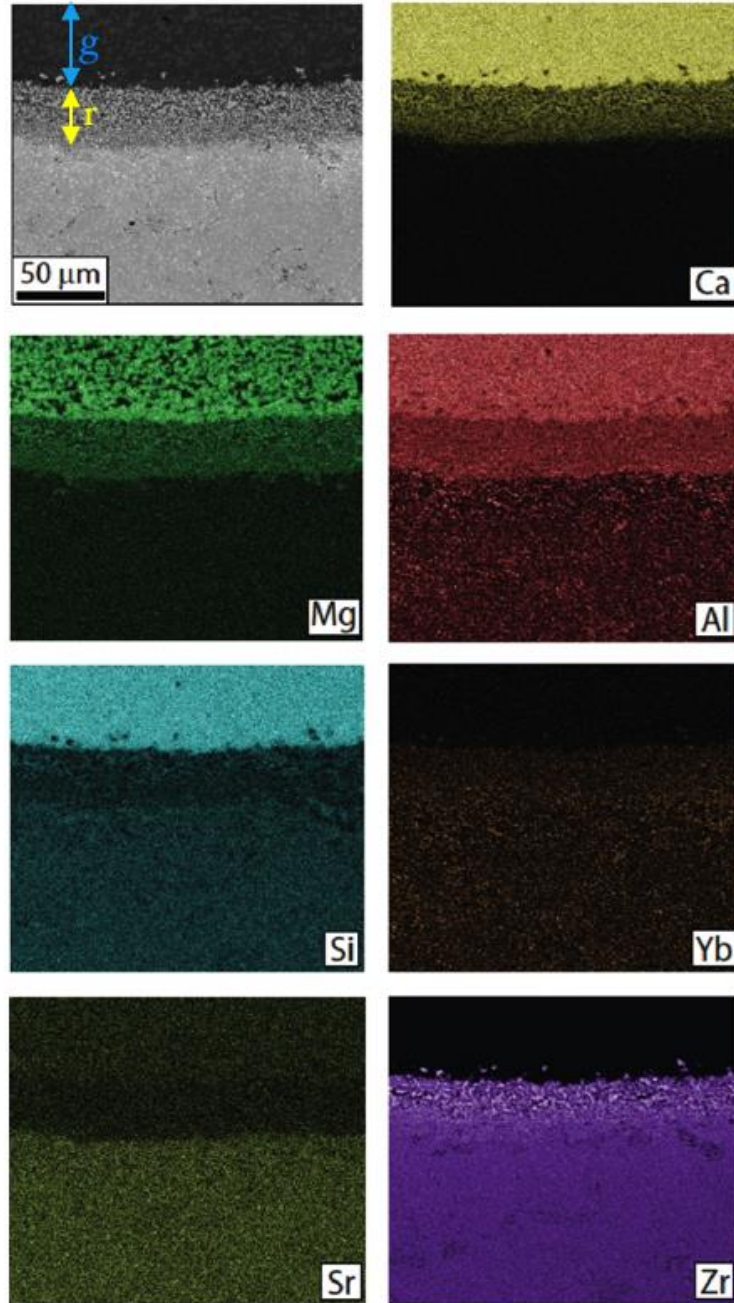
Figure 10. EDS mapping results from the 5Yb-SZ specimen.

Conclusion

The various results related to the infiltration of CMAS in atomic scale encourage contemplating the ionic diffusion contingent upon heat and vacancy. In order to make a distinct classification among the six oxide compositions studied, three possibilities may emerge:

    i.   the oxide can precipitate into the glass formed by CMAS and is not well bonded, which is the case for $LaPO_4$,

   ii.   the oxide can block the glass penetration by forming a dense layer, which is the case for mullite, GZO, GYZO, and Yb-SZ,

   iii.   the oxide can completely react with CMAS precipitating other phases such as anorthite, diopside, which is the case for 4YSZ.

CMAS reactivity with the oxides that are potential candidates for the next generation thermal barrier coatings was evaluated via SEM and EDS characterization, generating the following results:

1. The results have shown that 4YSZ quickly undergoes a complete phase transformation yielding different structures, expected to be anorthite and diopside. No glassy phase was observed within the structure in contrast with the case in EB-PVD deposited columnar structures.

2. Recently suggested pyrochlore zirconate structures such as $Gd_2Zr_2O_7$ and $GdYbZr_2O_7$ yielded promising results in terms of having high resistance to CMAS attacks.

3. Small dopants of lanthanide oxides were found to be changing the thermomechanical properties of some perovskite structures drastically. 5Yb-SZ gives outstanding results in terms of mitigating the glassy phase infiltration by forming a dense zirconate layer at the glass/crystal interface.

4. The mullite sample served as a potent oxygen barrier, and penetration of CMAS into the mullite scarcely took place forming anorthite crystals in the glass. However, due to low thermal expansion of mullite, delaminations will prolly develop parallel to the surface during service. Its potential use in TBCs may be limited on account of this attribute of mullite.

5. In most ceramic oxide systems including zirconium, ZrO_2 rich particles have shown tendency to spheroidize in the liquid phase when CMAS is introduced, probably because of its surface energy.

Acknowledgments

superb electron microscopy skills in taking the SEM images and EDS mapping and Randall C. Schubert for his advanced machinery skills in drilling the divots on infiltration specimens.

REFERENCES

[1] Bathie W., Fundamentals of Gas Turbines 2nd ed, John Wiley&Sons, 1996.

[2] Padture N.P., Gell M., Jordan E.H., Thermal Barrier Coatings for Gas-Turbine Engine Applications. Science, 2002. 296: p. 280-284.

[3] Jones R.L., Metallurgical and Ceramic Protective Coatings, ed: K. H. Stern, 1st ed, Chapman and Hall, London, 1996. p. 194.

[4] Pollock T.M., Tin S., Nickel-Based Superalloys for Advanced Turbine Engines: Chemistry, Microstructure, and Properties. Journal of Propulsion and Power, 2006. 22 [2]: p. 361-374.

[5] Miller R.A., Current Status of Thermal Barrier Coatings – An Overview, Surface and Coatings Technology, 1987. 30: p. 1-11.

[6] Levi C.G., Emerging materials and processes for thermal barrier systems. Current Opinion in Solid State and Materials Science, 2004. 8: p.77-91.

[7] Limarga A.M., Vaßen R., Clarke D.R., Stress Distributions in Plasma-Sprayed Thermal Barrier Coatings Under Thermal Cycling in a Temperature Gradient. Journal of Applied Mechanics, 2011. 78: 011003-1-9.

[8] Heeg B., Tolpygo V.K., Clarke D.R., Damage Evolution in Thermal Barrier Coatings with Thermal Cycling. Journal of the American Ceramic Society, 2011. 94 [1]: p. 112-119.

[9] Wellman R.G., Nicholls J.R., Erosion, corrosion, and erosion-corrosion of EB PVD thermal barrier coatings. Tribology International, 2008. 41: p: 657-662.

[10] Ruud J.A., Bartz A., Borom M.P., and Johnson C.A., Strength Degradation and Failure Mechanisms of Electron-Beam Physical-Vapor-Deposited Thermal Barrier Coatings. Journal of the American Ceramic Society, 2001. 84 [7]: p. 1545-52.

[11] Portinha A., Teixeira V., Carneiro J., Beghi M.G., Bottani C.E., Franco N., Vaßen R., Stöver D., Sequeira A.D., Residual Stresses and elastic modulus of thermal barrier coatings graded in porosity. Surface & Coatings Technology, 2004. 188-189: p: 120-128.

[12] Shillington E. A., Clarke D.R., Spalling Failure of a Thermal Barrier Coating Associated with Aluminum Depletion in The Bond-Coat. Acta Materialia, 1999. 47 80 [4]: p. 1297-1305.

[13] Guo H., Gong S., Xu H., Evaluation of hot-fatigue behaviors of EB-PVD gradient thermal barrier coatings. Materials Science and Engineering A, 2002. 325: p. 261- 269.

[14] Mumm D.R., Evans A.G., Spitsberg I.T., Characterization of a Cyclic Displacement Instability for a Thermally Grown Oxide in a Thermal Barrier System. Acta Materialia, 2001. 49: p. 2329-2340.

[15] Evans A.G., Mumm D.R., Hutchinson J.W., Meier G.H., Pettit F.S., Mechanisms controlling the durability of thermal barrier coatings. Progress in Materials Science, 2001. 46: p. 505-553.

[16] Garvie R.C., Hannink R.H., Pascoe R.T., Ceramic Steel. Nature, 1975. 258 [5537]: p. 703-704.

[17] Liebert et al., Durability of zirconia thermal-barrier ceramic coatings on air-cooled turbine blades in cyclic jet engine operation. NASA Tech. Memo., (1976). X-3410.

[18] Stecura S., Two-layer thermal barrier coating for turbine airfoils — furnace and burner rig test results. NASA Tech. Memo., 1976. X-3425.

[19] Zhong X.H., Wang Y.M., Xu Z.H., Zhang Y.F., Zhang J.F., Cao X.Q., Hot-corroion behaviors of overlay-clad yttria-stabilized zirconia coatings in contact with vanadate-sulfate salts. Journal of the European Ceramic Society, 2010. 30: p. 1401- 1408.

[20] Clarke D.R., Materials selection guidelines for low thermal conductivity thermal barrier coatings. Surface and Coatings Technology, 2003. 163-164: p. 67-74.

[21] Krämer S., Yang J., Levi C.G, Thermochemical Interaction of Thermal Barrier Coatings with Molten CaO-MgO-Al2O3-SiO2 (CMAS) Deposits. Journal of the American Ceramic Society, 2006. 89 [10]: p. 3167-3175.

[22] Borom M.P., Johnson C.A., Peluso L.A., Role of environmental deposits and operating surface temperature in spallation of air plasma sprayed thermal barrier coatings. Surface and Coatings Technology, 1996. 86-87: p. 116-126.

[23] Mercer C., Faulhaber S., Evans A.G., Darolia R., A delamination mechanism for thermal barrier coatings subject to calcium-magnesium-alumino-silicate (CMAS) infiltration. Acta Materialia, 2005. 53 [4]: p. 1029-1039.

[24] Krämer S., Faulhaber S., Chambers M., Clarke D.R., Levi C.G., Hutchinson J.W., Evans A.G., Mechanisms of cracking and delamination within thick thermal barrier systems in aero-engines subject to calcium-magnesium-alumino-silicate (CMAS) penetration. Materials Science and Engineering A, 2008. 490: p. 26-35.

[25] Li L., Hitchman N., Knapp J., Failure of Thermal Barrier Coatings Subjected to CMAS Attack. Journal of Thermal Spray Technology, 2010. 19 [1-2]: p.148-155.

[26] Steinke T., Sebold D., Mack D.E., Vaßen R., Stöver D., A novel test approach for plasma-sprayed coatings tested simultaneously under CMAS and thermal gradient cycling conditions. Surface and Coatings Technology, 2010. 205: p. 2287-2295.

[27] Drexler J.M., Aygün A., Li D., Vaßen R., Steinke T., Padture N.P., Thermal-gradient testing of thermal barrier coatings under simultaneous attack by molten glassy deposits and its mitigation. Surface and Coatings Technology, 2010. 204: p. 2683- 2688.

[28] Mohan P., Patterson T., Yao B., Sohn Y., Degradation of Thermal Barrier Coatings by Fuel Impurities and CMAS: Thermochemical Interactions and Mitigation Approaches. Journal of Thermal Spray Technology, 2010. 19 [1-2]: p. 156-167.

[29] Gledhill A.D., Reddy K.M., Drexler J.M., Shinoda K., Sampath S., Padture N.P., 86 Mitigation of damage from molten fly ash to air-plasma-sprayed thermal barrier coatings. Materials Science and Engineering A, 2011. 528: p. 7214-7221.

[30] Chen X., Calcium–magnesium–alumina–silicate (CMAS) delamination mechanisms in EB-PVD thermal barrier coatings. Surface & Coatings Technology, 2006. 200: p. 3418– 3427.

[31] Harder B.J., Ramirez-Rico J.J., Almery J.D., Lee K.N., Faber K.T., Chemical and Mechanical Consequences of Environmental Barrier Coating Exposure to Calcium– Magnesium–Aluminosilicate. Journal of the American Ceramic Society, 2011. 94 [1]: p. 178–185.

[32] Mannich P., Braue W., Uwe Schulz U., High-Temperature Corrosion of EB-PVD Yttria Partially Stabilized Zirconia Thermal Barrier Coatings with an Artificial Volcanic Ash Overlay. Journal of the American Ceramic Society, 2011. 94 [3]: p. 925–931.

[33] Wu J., Guo H., Gao Y., Gong S., Microstructure and thermo-physical properties of yttria stabilized zirconia coatings with CMAS deposits. Journal of the European Ceramic Society, 2011. 31: p. 1881–1888.

[34] Krämer S., Yang J., Levi C.G., Infiltration-Inhibiting Reaction of Gadolinium Zirconate Thermal Barrier Coatings with CMAS Melts. Journal of the American Ceramic Society, 2008. 91 [2]: p. 576–583.

[35] Wellman R., Whitman G., Nicholls J.R., CMAS corrosion of EB PVD TBCs: Identifying the minimum level to initiate damage. International Journal of Refractory Metals & Hard Materials, 2010. 28: p. 124–132.

[36] Hannink, R.H.J., Kelly P.M., Muddle B.C., Transformation toughening in zirconia containing ceramics. Journal of the American Ceramic Society, 2000. 83 [3]: p. 461- 487.

[37] Krogstad J., Kramer K, Lipkin D.M., Johnson C.A., Mitchell D.R.G., Cairney J.M., Levi C.G., Phase Stability of *t'*-Zirconia-Based Thermal Barrier Coatings: Mechanistic Insights, Journal of The American Ceramic Society, 2011. 94 [S1] S168–S177 (2011).

[38] Vaßen R., Traeger F., Stöver D., New Thermal Barrier Coatings Based on Pyrochlore/YSZ Double-Layer Systems. International Journal of Applied Ceramic Technology, 2004. 1 [4]: p. 351-61.

[39] Cao X.Q., Vaßen R., Stöver D., Ceramic Materials for Thermal barrier coatings. Journal of the European Ceramic Society, 2004. 24: p. 1-10.

[40] Morgan P.E.D., Marshall D.B., Ceramic Composites of Monazite and Alumina. Journal of the American Ceramic Society, 1995. 78 [6]: p.1553-63.

[41] Girolamo G., Blasi C., Pilloni L., Schioppa M., Microstructural and thermal properties of plasma sprayed mullite coatings. Ceramics International, 2010. 36: p. 1389–1395.

[42] Nadler M.R., Fitzsimmons E.S., Preparation and Properties of Calcium Zirconate. Journal of the American Ceramic Society, 1955. 38 [6]: p. 214-217.

[43] Vishnevskii I.I., Skripak V.N., Thermal Conductivity of Some Oxygen Compounds of Zirconium and Hafnium. Refractories and Industrial Ceramics, 1970. 11 [11-12]: p. 693-694.

[44] $SrZrO_3$ Crystal Structure: Datasheet from "PAULING FILE Multinaries Edition – 2012" in SpringerMaterials (https://materials.springer.com/isp/crystallographic/docs/sd_0543582).

[45] Ma W., Mack D.E., Vaßen R., Stöver D., Perovskite-Type Strontium Zirconate as a New Material for Thermal Barrier Coatings. Journal of the American Ceramic Society, 2008. 91 [8]: p. 2630–2635.

[46] Geisler T., Schaltegger U., Tomaschek F., Re-equilibration of Zircon in Aqueous Fluids and Melts. Elements, 2007. 3: p. 43–50.

[48] Kaiser A., Lobert M., Telle R., Thermal stability of Zircon (ZrSiO4). Journal of the European Ceramic Society, 2008. 28: p. 2199–2211.

[49] Lehmann H., Pitzer D., Pracht G., Vaßen R., Stöver D., Thermal Conductivity and Thermal Expansion Coefficients of the Lanthanum Rare-Earth-Element Zirconate System. Journal of the American Ceramic Society, 2003. 86 [8]: p. 1338-44.

[50] Liu Z., Ouyang J., Zhou Y., Li J., Xia X., Densification, Structure, and Thermophysical Properties of Ytterbium–Gadolinium Zirconate Ceramics. International Journal of Applied Ceramic Technology, 2009. 6 [4]: p. 485–491.

[51] Ma W., Mack D., Malzbender J., Vaßen R., Stöver D., Yb_2O_3 and Gd_2O_3 doped strontium zirconate for thermal barrier coatings. Journal of the European Ceramic Society, 2008. 28: p.3071–3081.

[52] Ahlborg N.L., Zhu D., Calcium-Magnesium-Aluminosilicate (CMAS) Reactions and Degradation Mechanisms of Advanced Environmental Barrier Coatings, NASA/TM—2013-218091paper prepared for the 40th International Conference on Metallurgical Coatings and Thin Films (ICMCTF 2013), Glenn Research Center Cleveland, Ohio 44135, November 2013.

[53] Schulz U., Braue W., Degradation of $La_2Zr_2O_7$ and other novel EB-PVD thermal barrier coatings by CMAS ($CaO–MgO–Al_2O_3–SiO_2$) and volcanic ash deposits, Surface & Coatings Technology 235 (2013) 165–173.

[54] Steinke T., Sebold D., Mack D.E., Vaßen R., Stöver D., A novel test approach for plasma-sprayed coatings tested simultaneously under CMAS and thermal gradient cycling conditions. Surface and Coatings Technology, 2010. 205: p. 2287-2295.